MOLECULAR IMAGING AND BIOLOGY

Mol Imaging Biol (2019) 21:747–757
DOI: 10.1007/s11307-018-1289-5

Published Online: 25 October 2018

RESEARCH ARTICLE

Predicting Glioblastoma Response to Bevacizumab Through MRI Biomarkers of the Tumor Microenvironment

Andreas Stadlbauer,[1,2] Karl Roessler,[1] Max Zimmermann,[1] Michael Buchfelder,[1] Andrea Kleindienst,[1] Arnd Doerfler,[3] Gertraud Heinz,[2] Stefan Oberndorfer[4]

[1]*Department of Neurosurgery, University of Erlangen-Nürnberg, Schwabachanlage 6, 91054, Erlangen, Germany*
[2]*Institute of Medical Radiology, University Clinic of St. Pölten, Dunant-Platz 1, 3100, St. Pölten, Austria*
[3]*Department of Neuroradiology, University of Erlangen-Nürnberg, Schwabachanlage 6, 91054, Erlangen, Germany*
[4]*Department of Neurology, University Clinic of St. Pölten, Dunant-Platz 1, 3100, St. Pölten, Austria*

Abstract

Purpose: Glioblastoma (GB) is one of the most vascularized of all solid tumors and, therefore, represents an attractive target for antiangiogenic therapies. Many lesions, however, quickly develop escape mechanisms associated with changes in the tumor microenvironment (TME) resulting in rapid treatment failure. To prevent patients from adverse effects of ineffective therapy, there is a strong need to better predict and monitor antiangiogenic treatment response.
Procedures: We utilized a novel physiological magnetic resonance imaging (MRI) method combining the visualization of oxygen metabolism and neovascularization for classification of five different TME compartments: necrosis, hypoxia with/without neovascularization, oxidative phosphorylation, and aerobic glycolysis. This approach, termed TME mapping, was used to monitor changes in tumor biology and pathophysiology within the TME in response to bevacizumab treatment in 18 patients with recurrent GB.
Results: We detected dramatic changes in the TME by rearrangement of its compartments after the onset of bevacizumab treatment. All patients showed a decrease in active tumor volume and neovascularization as well as an increase in hypoxia and necrosis in the first follow-up after 3 months. We found that recurrent GB with a high percentage of neovascularization and active tumor before bevacizumab onset showed a poor or no treatment response.
Conclusions: TME mapping might be useful to develop strategies for patient stratification and response prediction before bevacizumab onset.

Key words: Glioblastoma, Bevacizumab, Antiangiogenic therapy, Recurrence, Treatment monitoring, Treatment failure, Tumor microenvironment, Hypoxia, Angiogenesis

Introduction

Glioblastoma (GB) is the most aggressive primary brain tumor in adults. Despite multimodal treatment involving neurosurgery, radiotherapy, and chemotherapy, no curative treatment is currently available [1] and the median life expectancy of affected patients is less than 15 months [2]. GB is characterized by a significant intratumoral heterogeneity including necrotic

Electronic supplementary material The online version of this article (https://doi.org/10.1007/s11307-018-1289-5) contains supplementary material, which is available to authorized users.

Correspondence to: Andreas Stadlbauer; *e-mail:* andi@nmr.at

and hypoxic areas as well as regions showing extensive invasion into the brain parenchyma or high proliferation rate with an elevated expression of vascular endothelial growth factor (VEGF) protein. VEGF has been identified as a critical regulator of tumor neovascularization, endothelial cell proliferation, and migration [3]. GB is therefore an attractive target for antiangiogenic therapies [4], and the VEGF-specific antibody bevacizumab was approved by the Food and Drug Administration (FDA) for this purpose in 2009 [5].

Anti-VEGF agents including bevacizumab have been shown to rapidly decrease vascular permeability of tumor vessels associated with a normalization of vascular architecture. This commonly results in high radiological response rates of 25 to 60 % [5–7] due to a marked decrease of contrast enhancement, hyperperfusion, and edema [6, 8]. Therefore, apparent responses to antiangiogenic therapy may be not necessarily indicative of a true antiglioma effect, and radiological response assessment should be interpreted with caution even though its criteria have been updated by the Response Assessment in Neuro-Oncology (RANO) working group [9, 10].

Clinical trials of bevacizumab in recurrent GB have shown a prolongation of progression-free survival, but the impact of this therapy on overall survival remains unclear [11, 12]. Responding patients typically have an initial short-term benefit, but unfortunately, these tumors continue to progress [12]. The reason is that bevacizumab has been associated with a number of changes in the tumor microenvironment (TME) such as secretion of angiogenic cytokines or lowering of oxygen levels [4, 13]. Hypoxia is thought to induce alternative angiogenic growth factors (*e.g.,* fibroblast growth factor 2) [14, 15], which replace VEGF in the interaction between tumor and endothelial cells and may even directly stimulate neovascularization [13]. De Groot *et al.* [16] showed that prolonged, continuous antiangiogenic therapy can result in increased tumor hypoxia, and GB may develop a shift to a predominantly infiltrative phenotype upon treatment with bevacizumab. Preclinical studies demonstrated, however, that a hypoxic TME appears to favor a metabolic switch in tumor cells towards an increased glycolysis [4, 17].

These compartments present specific niches (*i.e.,* vascular and hypoxic niches) within the TME which are emerging as critical regulators of cancer progression and therapeutic response in GB [18, 19]. Accumulating evidence suggests that intratumoral heterogeneity and divergent development of the TME within the same tumor are probably the keys for understanding treatment failure [20–23]. Thus, there is a need for noninvasive *in vivo* investigation of the TME heterogeneity in order to determine adequately or even predict a treatment response to antiangiogenic agents. Issues of invasiveness (electrodes) as well as limitations in access ($[^{15}O]O_2$ positron emission tomography (PET)) or low spatial resolution (near-infrared spectroscopy, NIRS) make the existing techniques impractical for *in vivo* characterization in humans. A novel multiparametric MRI approach (termed "TME mapping") has been introduced recently, which allows for classification of the TME and detection of tumor-supportive hypoxic and vascular niches in GB patients [24]. TME mapping enables the assessment of the dominant metabolic strategy for energy production and uncovers two survival-relevant metabolic phenotypes of GB. In this study, we used this MRI approach and hypothesized that TME mapping provides insight into pathophysiological mechanisms of bevacizumab and furthermore predicts the treatment response in patients with recurrent GB.

Materials and Methods

Patients

Reviewing our institutional databases, we identified patients with GB World Health Organization (WHO) grade IV meeting the following inclusion criteria: (i) aged > 18 years; (ii) pathologically confirmed GB based on the WHO histological grading system; (iii) recurrence of the tumor after treatment according to standard of care (maximal safe resection, radiotherapy, and concomitant and adjuvant chemotherapy with temozolomide) [2]; (iv) recurrence was determined by at least two board-certified radiologists in consensus based on the updated RANO criteria [9, 10] with clear radiological features of recurrence; (v) bevacizumab (Avastin®, Roche; every 2 weeks 10 mg/kg-bodyweight) as second-line mono-therapy of the recurrent GB; and (vi) MRI data using our study MRI protocol available at recurrence and follow-up MRI examinations. This retrospective analysis was approved by the institutional ethics committee of the University of Erlangen and the University Clinic of St. Pölten, and all patients gave their written informed consent permitting scientific work with clinical data and MRI scans.

MRI Data Acquisition

MRI examinations were performed 1–5 days prior to (pre-bevacizumab) as well as 3 and 6 months after bevacizumab treatment onset (follow-up 1 and 2), respectively, on a 3 Tesla clinical scanner (Tim Trio, Siemens, Erlangen, Germany) equipped with a standard 12-channel head coil. The MRI protocol included the following sequences: axial fluid–attenuated inversion-recovery (FLAIR; TR/TE/TI, 5000/460/1800 ms; in-plane resolution, 0.45×0.45 mm; slice thickness, 3 mm); a single-shot diffusion-weighted echo-planar imaging (DW-EPI) sequence (TR/TE, 5300/98 ms; in-plane resolution, 1.2×1.2 mm; slice thickness, 4 mm; 29 slices, b values of 0 and 1000 s/mm^2); and pre- and post-contrast-enhanced T1-weighted gradient-echo MRI sequences (TR/TE, 250/2.8 ms; in-plane resolution, 0.5×0.5 mm; slice thickness, 4 mm; 29 slices).

For oxygen metabolism, we used the multiparametric quantitative blood oxygen level-dependent imaging

(qBOLD) approach, which required (i) a multi-echo gradient echo (GE) sequence for R2*-mapping (8 echoes; TE, 5–40 ms), and (ii) a multi-echo spin echo (SE) sequence for R2-mapping (8 echoes; TE, 13–104 ms) was performed, respectively.

For neovascularization, we used the vascular architecture mapping (VAM) approach, which required a dynamic susceptibility contrast (DSC) perfusion MRI data obtained with SE (TR, 1740 ms; TE, 33 ms) and GE (TR, 1740 ms; TE, 22 ms) EPI sequences, respectively, using dual contrast agent injections [25–27]. Sixty dynamic measurements were used for both DSC perfusion experiments in combination with the injection of 0.1 mmol/kg-bodyweight gadoterate-meglumine (Dotarem, Guerbet) with a flow of 4 ml/s *via* a MR-compatible injector (Spectris, Medrad) followed by a 20-ml bolus of saline. Methods to minimize patient motion artifacts as well as variations in the contrast media bolus passage that could massively impair data post-processing were published previously [26, 27]. In order to allow for calculations during data post-processing, all five MRI sequences (DW-EPI, R2*-mapping, R2-mapping, SE- EPI DSC, and GE-EPI DSC) had the same geometric parameters: 1.8×1.8 mm; slice thickness, 4 mm; 29 slices. The time additional required for the qBOLD (R2*-mapping and R2-mapping) and VAM sequences (SE-EPI DSC) was 7 min.

MRI Data Processing

Processing of qBOLD and VAM data, and calculation of MRI biomarker maps for oxygen metabolism and neovascularization, was performed with custom-made MatLab (MathWorks, Natick, MA) software. Details about the whole data processing pipeline from MRI data acquisition over pre-processing to biomarker calculation are shown online in the Electronic Supplementary Materials (ESM, Suppl. Fig. 1). Both, qBOLD and VAM data processing, consisted of three steps.

The qBOLD data processing: (i) Corrections for background fields of the R2*-mapping data20 and for stimulated echoes of the R2-mapping data [28]; (ii) calculation of R2*-maps and R2-maps from the multi-echo MR-relaxometry data; and (iii) calculation of absolute cerebral blood volume (CBV) and flow (CBF) maps from the GE-EPI DSC perfusion MRI data *via* automatic identification of arterial input functions (AIFs) [29, 30]. These data were used for calculation of MRI biomarker maps of oxygen metabolism, including oxygen extraction fraction (OEF), cerebral metabolic rate of oxygen ($CMRO_2$) [31], and the average mitochondrial oxygen tension ($mitoPO_2$), as described previously [32, 33].

The VAM data processing was described in detail previously [25, 27]. Briefly, it consisted of (i) correction for remaining contrast agent extravasation [34, 35]; (ii) fitting of the first bolus curves for each voxel of the GE-DSC and SE-DSC perfusion data with gamma-variate function [36]; and (iii) calculation of the $\Delta R_{2,GE}$*versus* $(\Delta R_{2,SE})^{3/2}$ diagram [37]—the so-called vascular hysteresis loop (VHL). These data were used for calculation of MRI biomarker maps of neovascularization, including the microvessel type indicator (MTI) and the upper limit of microvessel density (N_U) and radius (R_U) [38].

Tumor Microenvironment Mapping

The TME mapping approach consisted of four steps [24]. (i) classification of the oxidative status in mitochondria; (ii) classification integrity of the tumor neovasculature; (iii) fusion of this classified information in one imaging data set; and (iv) classification of TME compartments within this data set including and considering the $CMRO_2$-OEF-scatterplot (see bottom of Suppl. Fig. 1 in ESM and the corresponding figure caption for a more detailed discussion). This procedure was associated with the introduction of five different TME compartments for oxygen metabolism and neovascularization [24]. The criteria for classification of the TME compartments are listed in Table 1.

The voxels of each TME compartment were assigned with different colors (rightmost column in Table 1) which resulted in the so-called oxygen metabolism-neovascularization TME map. Additionally, the total tumor volume with neovascularization was calculated as the sum of the TME compartments hypoxia with NV, OxPhos, and glycolysis, respectively. The active tumor volume was the sum of OxPhos and glycolysis.

Quantitative and Statistical Analysis

For quantitative analysis of the TME, regions of interest (ROIs) were manually defined by experienced neuroradiologist and medical physicist in consensus based on features seen in both the contrast-enhanced T1-weighted and FLAIR images. The ROIs were transferred to the TME maps, and the volumes of the five TME compartments were calculated. Follow-up MRI examinations were evaluated using the modified RANO criteria [9, 10]. In short, (i) progressive disease defined as ≥ 25 % increase in the bidimensional product; (ii) stable disease as < 50 % decrease to < 25 % increase; and (iii) partial response ≥ 50 % decrease.

The Software (SPSS 21, IBM, Chicago, IL, USA) was used for statistical evaluation. Differences in the five TME compartments (necrosis, hypoxia with/without neovascularization, OxPhos, glycolysis) and the total neovascularized tumor volume over the course of all three examinations (baseline, follow-ups 1 and 2) as well as between the three patient subgroups (progression, stable disease, and partial response) were determined by using analysis of variance (ANOVA). The Dunnett T3 test was used as a *post hoc* procedure to be consistent with the assumption that homogeneity of variance was not met and for correction for multiple comparisons. Homogeneity of variance was tested by using the Levene test. *P* values less than 0.05 were

Table 1.. Criteria for classification of TME compartments

$mitoPO_2$ limit (mmHg)	$CMRO_2$ range (μmol/100 g min)	OEF range (%)	MIT limit ($s^{-5/2}$)	NU limit (mm^{-2})	Interpretation	Abbreviation	Voxel color in TME map
< 10	> 80 < 150	> 50	> − 5.0 < 5.0	< 250	Hypoxia with dysfunctional NV	Hypoxia, no NV	Red
< 10	> 150	< 50	< − 5.0 > 5.0	> 250	Hypoxia with functional NV	Hypoxia + NV	Yellow
10–60	< 130	> 75	> − 5.0 < 5.0	< 250	Necrosis with highly defective vasculat.	Necrosis	Black
10–60	> 70	< 50	< − 5.0 > 5.0	> 250	Normoxic tumor with functional NV	OxPhos + NV	Green
> 60	< 150	< 20	< − 5.0 > 5.0	> 250	Energy prod. without mitochondrial involv.	Glycolysis + NV	Blue

$mitoPO_2$, mitochondrial oxygen tension; *$CMRO_2$*, cerebral metabolic rate of oxygen; *OEF*, oxygen extraction fraction; *MTI*, microvessel type indicator; *N_U*, microvessel density; *NV*, neovascularization; *TME*, tumor microenvironment

considered to indicate significance. We performed Kaplan-Meier survival analysis with the log-rank test on categorical clinical variables, including age ≥ 60 years, KPS ≤ 80, extent of resection (EOR), gender, and patient subgroups.

Post-operative MRI examinations (48 h after surgery) were used for determination of EOR. Resection of more than 95 % of the enhancing tumor was defined as "cross total resection" or else (≤ 95 % of the enhancing tumor) as "subtotal resection." Survival after progression (SAP) was the time period between diagnosis of progression and death. Radiologic progression was determined by two experienced radiologists in consensus using the updated RANO criteria. Clear radiological features of recurrence were required [9, 10]. Overall survival (OS) was the time period between initial diagnosis and death. Patients who were alive at last contact were censored for analysis of both SAP and OS. Statistically significant ($P < 0.05$) factors in univariate analysis were considered in the multivariate survival analysis using the Cox proportional hazard ratio (HR) model for assessment of the association between the metabolic phenotypes with SAP and OS.

Results

Patient Characteristics and Subgroups

A total of 18 patients (9 men, 9 women; mean age 55.6 ± 12.8 years) with recurrent GB satisfied the inclusion criteria and received overall 49 MRI scans with our study protocol between July 2015 and June 2018. Six patients had a Karnofsky performance score (KPS) of 80 or below; the median KPS was 95 at diagnosis of recurrence. Median overall survival (OS) and survival after progression (SAP) was 633 and 254 days, respectively; six patients (33 %) still alive at last contact were censored.

Analysis of conventional MRI data (including CE T1w and FLAIR) revealed the following three clinical patterns assessed with the modified RANO criteria: (i) *Progression* of the GB during bevacizumab treatment was observed in five patients. In three of them, only one follow-up MRI (3 months after treatment onset) was possible because of the death of the patients. (ii) Another five patients demonstrated *stable disease* in the first follow-up MRI. Two of them died before the second follow-up MRI, and the remaining three patients demonstrated GB progression in the second follow-up MRI. (iii) Eight patients demonstrated a *partial response* to bevacizumab in the first follow-up MRI. This resulted in three patient subgroups regarding to the response to bevacizumab assessed with the modified RANO criteria. Patient characteristics of these three patient subgroups are summarized in Table 2.

Differences in the TME Between Subgroups

MRI biomarker maps of oxygen metabolism (OEF, $CMRO_2$, $mitoPO_2$) and neovascularization (MTI, N_U, R_U) were calculated, and TME mapping was successfully performed for all 18 MRI examinations before bevacizumab onset and for all 31 follow-up examinations of the 18 patients, respectively. All follow-up examinations demonstrated dramatic changes in the TME due to the antiangiogenic therapy.

In Fig. 1, conventional MRI, oxygen tension, neovascularization, and TME mapping are depicted for a GB patient with *progression* during bevacizumab treatment. Initially, in this recurrent GB, a high percentage of the tumor volume preferred glycolysis and OxPhos (*i.e.,* was active tumor) and a relative low percentage demonstrated necrosis and hypoxia before bevacizumab onset. Neovascularization (*i.e.,* the sum of hypoxia with NV, OxPhos and glycolysis) was also high with 69.6 % of the tumor. Following treatment, the neovascularized tumor volume only decreased approximately by half to 35.7 % but increased in the second follow-up again to 39.9 %. Similarly, the active tumor volume decreased from 68.8 to 30.2 % in the first 3 months after bevacizumab onset but started increasing again during the second 3 months of the therapy to 33.1 %. Moreover, the new development during this time period (infiltration into the contralateral hemisphere) preferred OxPhos and glycolysis. Another illustrative case of a patient with GB progression under bevacizumab treatment is shown in Suppl. Fig. 2 in the ESM.

Table 2. Patient characteristics

ID	Age	Gender	Histopathology	Location	KI	EOR	RANO
1	54.0	m	GB WHO IV, IDH wt	r, parietal	90	GTR	Stable dis.
2	51.1	m	GB WHO IV, IDH wt	r, frontal	100	STR	Progression
3	31.1	m	GB WHO IV, IDH mut	l, frontal	100	GTR	Stable dis.
4	34.0	f	GB WHO IV, IDH wt	l, frontal	80	GTR	Progression
5	61.3	m	GB WHO IV, IDH wt	r, temporal	80	GTR	Part. resp.
6	52.7	f	GB WHO IV, IDH wt	l, frontal	80	STR	Part. resp.
7	55.6	f	GB WHO IV, IDH wt	l, parietal	80	STR	Stable dis.
8	44.0	f	GB WHO IV, IDH wt	r, frontal	100	GTR	Part. resp.
9	63.7	f	GB WHO IV, IDH wt	l, frontal	100	STR	Part. resp.
10	76.7	m	GB WHO IV, IDH wt	l, frontal	100	GTR	Progression
11	65.6	m	GB WHO IV, IDH wt	l, parietal	100	STR	Progression
12	70.6	f	GB WHO IV, IDH wt	r, temporal	100	GTR	Stable dis.
13	63.2	f	GB WHO IV, IDH wt	r, parietal	75	STR	Part. resp.
14	44.1	m	GB WHO IV, IDH wt	l, parietal	100	GTR	Progression
15	44.1	m	GB WHO IV, IDH wt	r, frontal	100	GTR	Part. resp.
16	51.1	f	GB WHO IV, IDH wt	r, parietal	90	STR	Part. resp.
17	70.6	f	GB WHO IV, IDH mut	r, occipital	90	STR	Stable dis.
18	67.3	m	GB WHO IV, IDH wt	r, temporal	80	STR	Part. resp.

m, male; *f*, female; *GB*, glioblastoma; *IDH*, isocitrate dehydrogenase gene; *wt*, wild type; *mut*, mutated; *I*, left; *r*, right; *GTR*, gross total resection; *STR*, subtotal resection

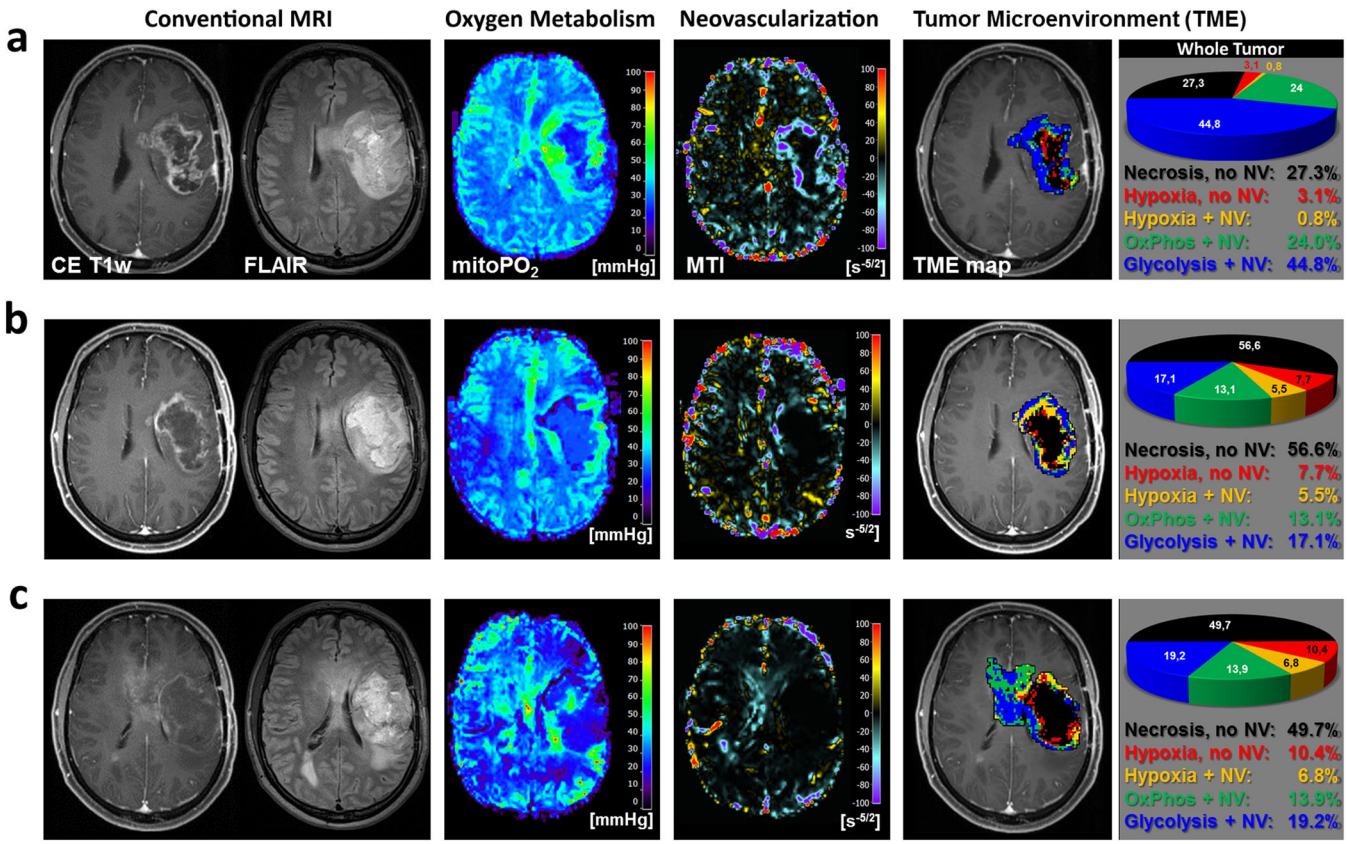

Fig. 1. Progression of recurrent GB following bevacizumab. Tumor microenvironment (TME) mapping of a patient (ID 14 in Table 2) suffering from recurrent GB **a** before bevacizumab onset, **b** at 3-month follow-up, and **c** at 6-month follow-up. This patient showed progression of the GB under bevacizumab treatment in the first follow-up. From left to right: conventional anatomic MRI (cMRI; gray box) including contrast-enhanced T1-weighted and FLAIR MRI; maps of mitochondrial oxygen tension ($mitoPO_2$) and microvessel type indicator (MTI) representing oxygen metabolism and neovascularization, respectively; results of TME mapping; and pie charts represent the percentages of TME compartments for the whole tumor volume.

In Fig. 2, an illustrative case showing *stable disease* in the first follow-up is demonstrated. This recurrent GB also showed a high percentage of active tumor volume and a relative low percentage of necrosis and hypoxia before bevacizumab onset. The active tumor volume decreased from 59.3 % by half to 28.6 % in the first 3 months after bevacizumab onset but increased during the second 3 months of therapy to 39.8 %. Similar to the patient with progression (Fig. 1), the tumor volume with neovascularization was initially high with 72.8 %, decreased following treatment initiation only to 39.7 %, and increased again to 52.3 % in the second follow-up. Another typical example for stable disease in the first follow-up is shown in Suppl. Fig. 3 in ESM.

In Fig. 3, the MRI examinations and TME mapping for a patient with *partial response* of the recurrent GB to bevacizumab treatment is depicted. This tumor showed a distinctly lower percentage for both active tumor (33.3 %) and neovascularization (49.2 %) before bevacizumab onset compared to the patients presented above. This was accompanied by a much larger necrotic and hypoxic tumor volume of the recurrent GB. Furthermore, during both the first and second 3 months of antiangiogenic treatment, the active tumor volume decreased substantially to 12.3 % and 6.7 %, respectively. Surprisingly, the neovascularized tumor volume decreased only slightly (to 38.7 %) during the first period but more strongly (to 16.1 %) during the second 3 months. The tumor volume is dominated by necrosis and hypoxia during the whole observation period. Another illustrative case with partial response under bevacizumab treatment is shown in Suppl. Fig. 4 in ESM.

Comparisons of the bevacizumab-naive TME (*i.e.,* before bevacizumab onset) between the three subgroups revealed that in GB with partial response, active tumor volume was initially significantly lower ($P = 0.039$ and 0.034), especially due to a lower percentage of OxPhos ($P = 0.008$ and 0.030). Furthermore, percentage of neovascularization was significantly lower ($P = 0.039$ and 0.034), and percentage of necrosis was significantly higher ($P = 0.001$ and 0.004) as compared to progression or stable disease, respectively. We found no significant differences between the two patient subgroups with progression and stable disease. In other words, recurrent GB with a TME that was initially dominated by neovascularization and active tumor (both >

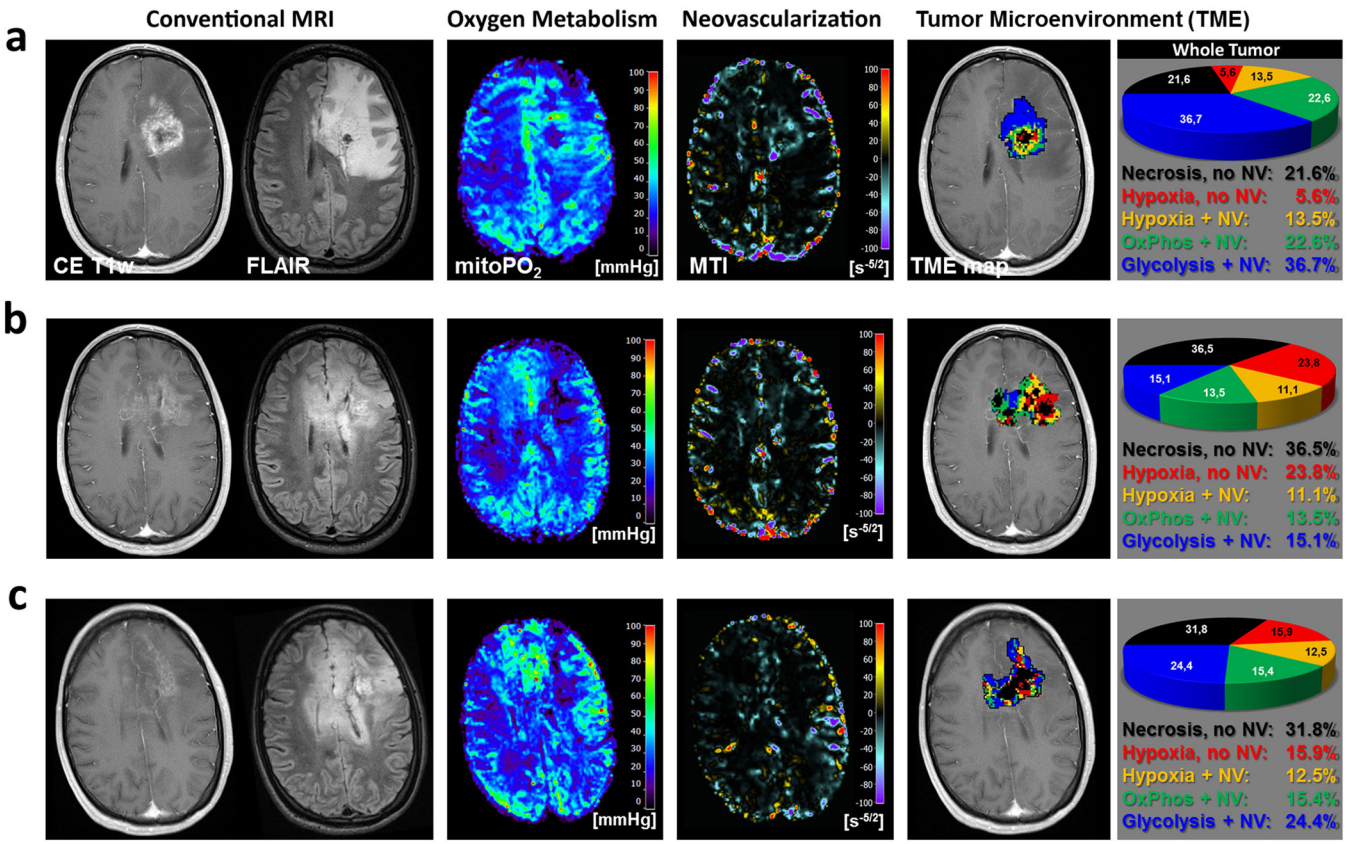

Fig. 2. Stable disease of recurrent GB following bevacizumab. Tumor microenvironment (TME) mapping a patient (ID 3) suffering from a recurrent GB **a** before bevacizumab onset, **b** at 3-month follow-up, and **c** at 6-month follow-up, respectively. This patient showed partial stable disease under bevacizumab treatment in the first follow-up. From left to right: conventional anatomic MRI (cMRI; gray box) including contrast-enhanced T1-weighted and FLAIR MRI; maps of mitochondrial oxygen tension ($mitoPO_2$) and microvessel type indicator (MTI) representing oxygen metabolism and neovascularization, respectively; results of TME mapping; and pie charts representing the percentages of TME compartments for the whole tumor volume.

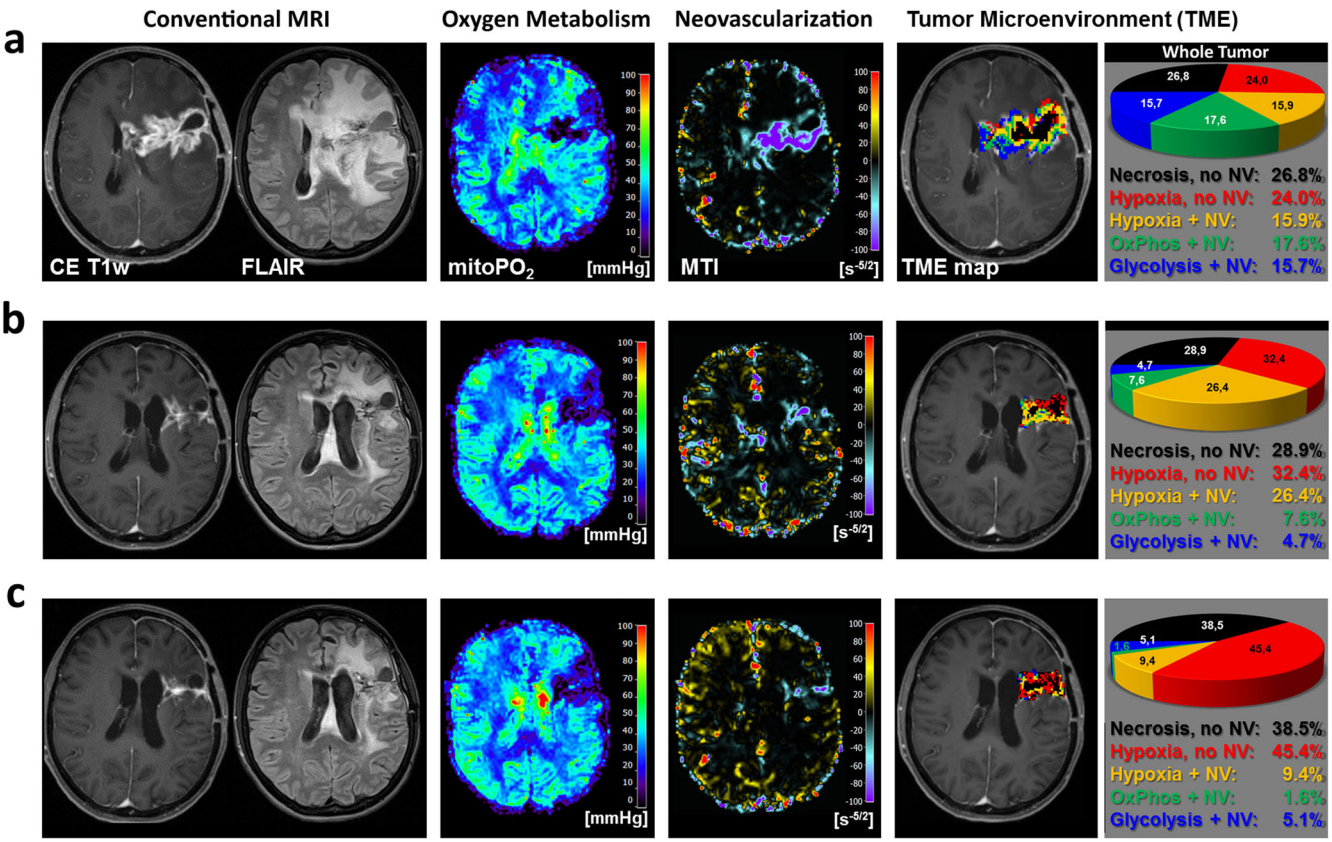

Fig. 3. Partial response of recurrent GB following bevacizumab. Tumor microenvironment (TME) mapping a patient (ID 6) suffering from a recurrent GB **a** before bevacizumab onset, **b** at 3-month follow-up, and **c** at 6-month follow-up, respectively. This patient showed partial response of the GB under bevacizumab treatment in the first follow-up. From left to right: conventional anatomic MRI (cMRI; gray box) including contrast-enhanced T1-weighted and FLAIR MRI; maps of mitochondrial oxygen tension ($mitoPO_2$) and microvessel type indicator (MTI) representing oxygen metabolism and neovascularization, respectively; results of TME mapping; and pie charts representing the percentages of TME compartments for the whole tumor volume.

50 % of the tumor volume) showed a poor or no response to a bevacizumab therapy.

Dynamic Changes in the TME and Survival Analyses

The time courses of the RANO parameter as well as the percentage of neovascularization and active tumor volume for the three patient subgroups are shown in Fig. 4. All three subgroups showed a significant decrease in both neovascularization and active tumor volume between the pre-bevacizumab MRI examination and the first follow-up, but not between the first and second follow-ups. However, the treatment effect on the TME is much stronger in the patient subgroup with a partial response: the tumor volume with neovascularization decreased relatively by 66.7 % from 49.6 to 16.5 % ($P < 0.001$), and the active tumor volume decreased relatively by 79.9 % from 38.7 to 7.8 % ($P < 0.001$) during the first 3 months. The treatment effects in the two other subgroups, which showed initially larger neovascularization and active tumor volume, were just half as strong and increased again in the second follow-up. This might be interpreted that the tumor burden in the poor and non-responding subgroups was too high for a stronger treatment effect in the first follow-up and consequently remained too high to achieve a longer lasting positive effect at the second follow-up. Therefore, the subgroup with a partial response showed a significant longer SAP compared to the other subgroups (progression, $P = 0.002$; stable disease, $P = 0.045$) but showed no significant differences in OS (Fig. 4).

Figure 5 gives an overview of the dynamic changes of the individual TME compartments for the three subgroups. In progressive GB, OxPhos decreased significant ($P = 0.021$) in between the pre-bevacizumab MRI and the first follow-up. In patients with stable disease, however, the glycolytic tumor volume decreased significantly ($P = 0.012$) between pre-bevacizumab and the first follow-up and increased significantly ($P = 0.021$) between first and second follow-ups, respectively. In GB with partial response, glycolysis decreased significantly ($P = 0.042$) as well as OxPhos

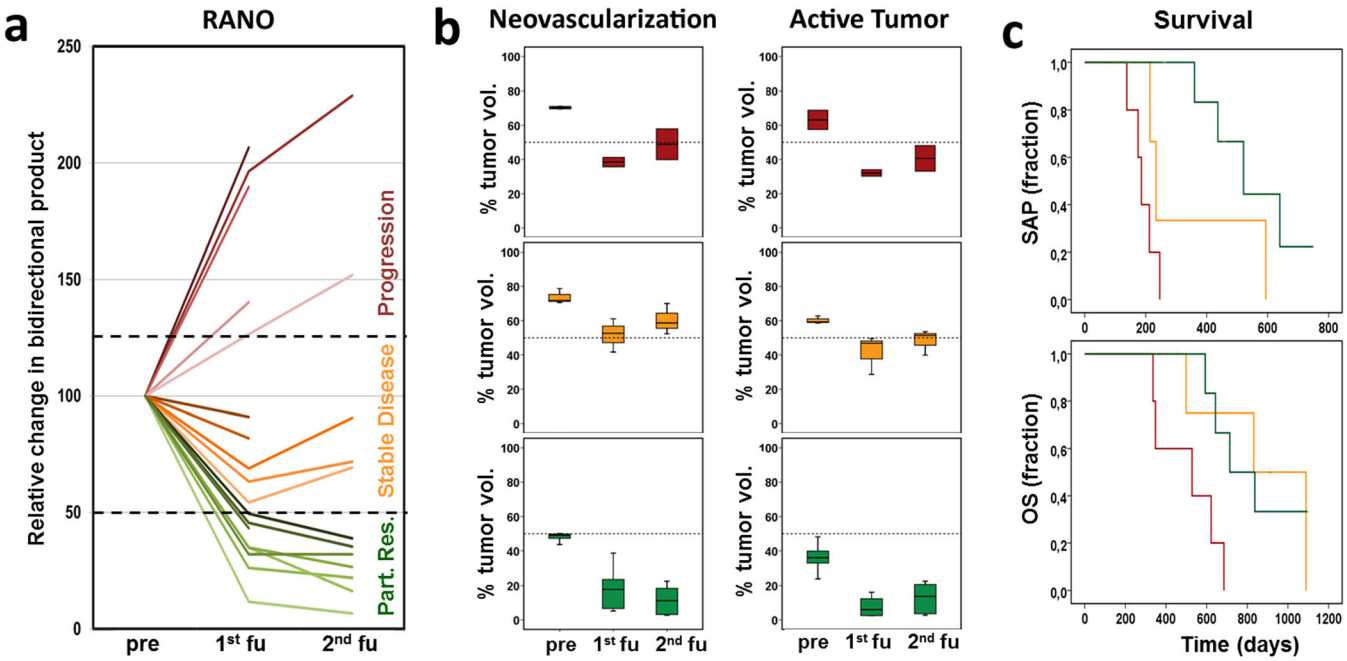

Fig. 4. Overview of radiological, tumor microenvironment, and survival data for the three patient subgroups: progression (red), stable disease (yellow), and partial response (green). From left to right: **a** Course of the radiological features (relative change in bidirectional product) in accordance with the modified RANO criteria, **b** percentage of tumor volume with neovascularization and active tumor volume. Rightmost: **c** Kaplan-Meier curves for survival after progression (SAP) and overall survival (OS) for the patient subgroups with progression (red lines), stable disease (yellow lines), and partial response (green lines), respectively. Pre, MRI examination before bevacizumab onset; 1st fu, first follow-up after 3 months; 2nd fu, second follow-up after 6 months.

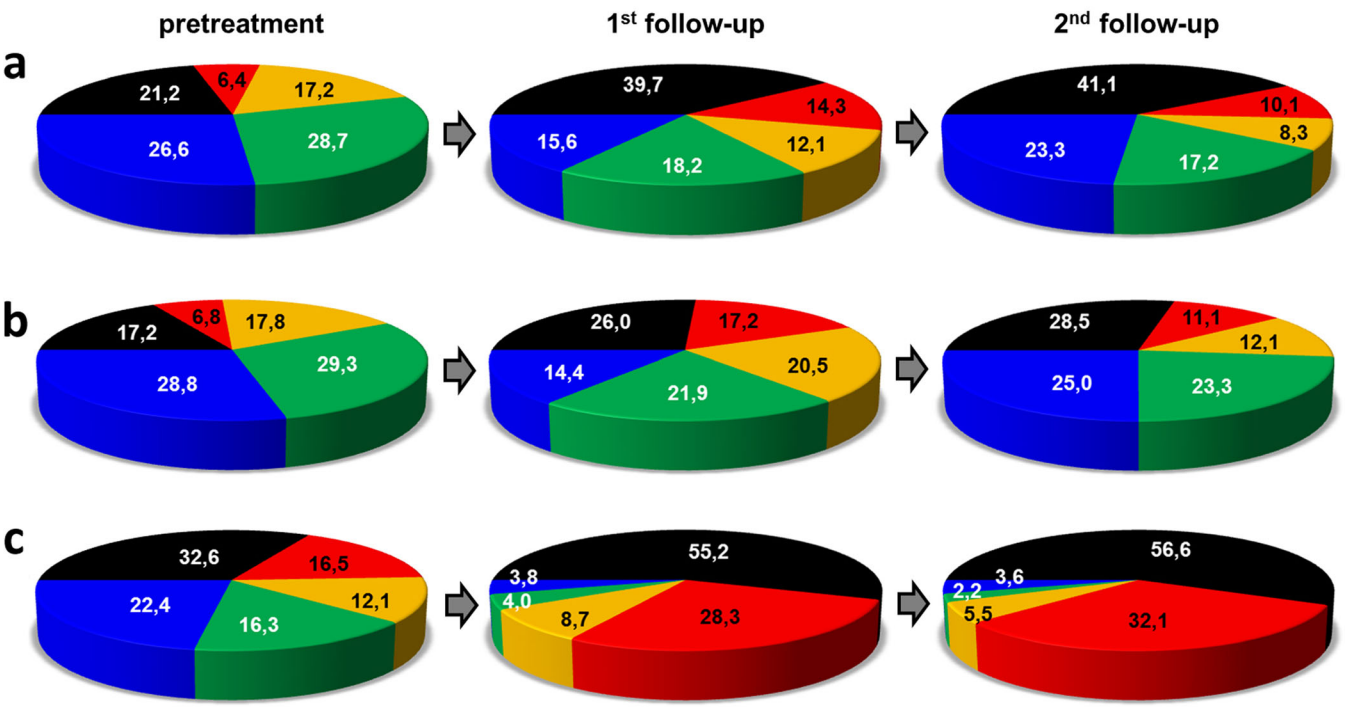

Fig. 5. Overview of the percentage of TME compartments for the three patient subgroups. Pie charts represent the percentages of TME compartments necrosis (black), hypoxia without neovascularization (red), hypoxia with neovascularization (yellow), OxPhos (green), and glycolysis (blue), respectively, for the whole tumor volume.

($P < 0.001$), while necrosis ($P = 0.009$) and hypoxia without neovascularization increased significantly ($P = 0.045$) between pre-bevacizumab and the first follow-up. Furthermore, which was very important for the patients with a partial response, these changes in the TME persisted at the second follow-up.

Discussion

GB is a highly vascularized tumor and, therefore, represents an attractive target for antiangiogenic therapies. Unfortunately, as observed on other cancers [39], the response to antiangiogenic therapy is almost always transient, and many tumors quickly develop escape mechanisms resulting in a rapid tumor progression [40, 41]. Thus, in order to prevent patients from adverse effects of an ineffective therapy, there is a strong need to monitor the pathophysiological mechanisms of antiangiogenic therapies better as well as to predict treatment response more precisely as early as possible—preferably before treatment onset.

In this study, we utilized TME mapping [24], a physiological MRI approach for combined detection of hypoxia and neovascularization, to monitor the bevacizumab treatment in patients with recurrent GB. Pre-bevacizumab TME mapping of recurrent GB revealed in all patients the same fundamental spatial structure and arrangement of the TME compartments which was similar to the known structure of newly diagnosed untreated GB [24]: a central necrosis was surrounded by a hypoxic TME compartment with defective vasculature and (still) functional neovasculature, respectively. This necrotic/hypoxic tumor core, in turn, was surrounded by TME compartments of active tumor relying predominantly on mitochondrial OxPhos or glycolysis, respectively, for energy production.

Follow-up examinations after bevacizumab initiation, however, demonstrated a dramatic rearrangement of the TME compartments. In all three patient subgroups, active tumor volume and neovascularization decreased, while hypoxia and necrosis were increased at the first follow-up. Both, the initial (bevacizumab-naive) TME structure and its changes during the first 3 months, were found to be of crucial importance for the treatment response and SAP. We found no significant differences in the TME between recurrent GB with progression or stable disease following bevacizumab therapy. In patients with partial response to bevacizumab, however, the TME was initially significantly different: these GB were more necrotic and had a lower percentage on active tumor and neovascularization before bevacizumab onset. In other words, highly vascularized and active GB showed a poor or no response to bevacizumab therapy probably due to a larger neovascular reserve, which requires a longer period of treatment for destruction of the neovasculature. Thereby, tumor cells in highly vascularized GB may have sufficient time to induce alternative angiogenic growth factors (*e.g.,* fibroblast growth factor 2) which replace VEGF and, consequently, enable these tumors to escape from treatment pressure using both the newly formed vascular and the increased hypoxic niche. In GB with an already defective neovasculature, however, bevacizumab results in a rapid, near-complete collapse of the tumor vasculature (and of the vascular niche), thereby increasing necrosis and hypoxia. Tumor cells, however, may survive in this remaining hypoxic niche and are the origin of recurrence and progression. This observation may help to develop strategies for response prediction of bevacizumab treatment based on noninvasive *in vivo* mapping of the TME.

Our findings of distinct alterations in the TME in response to bevacizumab treatment are in good agreement with previous studies in animal models investigating the tumor response to antiangiogenic therapy at the phenotypic, physiological, and molecular levels. Keunen *et al.* [4] used dynamic contrast-enhanced perfusion MRI in an intracranial GB xenograft model and found a significant decrease of the vascular supply because of a strong reduction of large- and medium-sized blood vessels in the tumors in response to bevacizumab. This was accompanied by an induction of hypoxia-inducible factor 1α, an activation of the phosphatidyl-inositol-3-kinase pathway, and a 68 % increase in infiltrating tumor cells in the brain parenchyma. The authors concluded that vascular remodeling induced by anti-VEGF treatment leads to a more hypoxic TME which favors a metabolic change of tumor cells towards glycolysis and promotes tumor invasiveness. Subsequent animal studies using multivoxel ^{1}H MR spectroscopy [42], [$^{13}C_6$]glucose metabolic flux analysis [17], and targeted proteomics [43], respectively, confirmed that an antiangiogenic treatment of GB increases tumor hypoxia and results in a metabolic adaptation towards glycolysis.

Here, we utilized a physiological MRI approach to directly investigate tumor hypoxia and neovascularization in humans and observed also an increase in hypoxia and necrosis in response to bevacizumab in all patients. Tumor glycolysis increased in GB patients who showed a tumor progression. However, we were able to identify a subgroup of patients who showed no re-increase of the glycolytic tumor volume but a partial response to bevacizumab, which might be helpful for response prediction and treatment planning.

A few studies described a noninvasive approach based on an advanced image analysis of multiparametric MRI data to predict the GB response to antiangiogenic treatment. Najafi *et al.* [44] described a method applying conventional MRI signal decomposition and histogram analysis to extract statistical signal features from contrast-enhanced tumor regions to assess the microstructural tumor characteristics. Changes in contrast-enhancement, necrosis (on CE T1w MRI), and edema (on FLAIR MRI) after treatment onset were used to evaluate the response. They observed significantly different shapes of the histograms between responders and non-responders and a strong correlation between the relative changes in the contrast-enhanced area and the necrotic area, respectively. Ellingson *et al.* [10] used

CE T1w subtraction maps to qualitatively enhance visualization and improve the quantification of tumor volume after bevacizumab treatment. They found that the CE T1w subtraction maps were significantly better at aiding prediction of 6-month progression-free survival (PFS) and 12-month OS compared with conventional tumor segmentation. Nowosielski *et al.* [45] and Rahman, *et al.* [46] investigated changes in the tumor tissue diffusivity *via* histogram analysis of apparent diffusion coefficient (ADC) maps in the course of antiangiogenic treatment of recurrent GB. They demonstrated that ADC histogram analysis within both enhancing and non-enhancing tumor components can be used to stratify for PFS and OS in patients with recurrent GB under antiangiogenic therapy. However, none of these studies assessed hypoxia which, as mentioned above, plays a key role in the antiangiogenic treatment response and failure. Furthermore, their predictions were based on differences in MRI features between baseline and post-treatment examinations. Here, we described a potential tool of patient stratification before bevacizumab onset.

However, our study has several limitations. Biological validation of the MR-based parameters for mitoPO_2, $CMRO_2$, hypoxia, and neovascularization is required by correlation with findings from immunohistochemistry, invasive methods, or other imaging modalities (*e.g.,* PET). The patient numbers especially in the subgroups with progression and stable disease were very small ($N = 5$). Furthermore, we did not include MRI examinations for both early response assessment (after 1 week or month) and long-term follow-up (after 1 year or more). Therefore, no strong conclusions can be drawn based on the results presented in this study. This study is the result of a retrospective analysis using a newly developed physiologic MRI approach, and further studies are required using this MRI technique to investigate early and long-term changes in larger patient populations.

Funding Information. This work was supported by the German Research Foundation (Deutsche Forschungsgemeinschaft—DFG; Grant Numbers STA 1331/3-1 and DO 721/9-1) and by the ELAN program (Erlanger Leistungsbezogene Anschubfinanzierung und Nachwuchsförderung; Grant Number 14-05-21-1-Stadlbauer).

Compliance with Ethical Standards

Conflict of Interest

The authors declare that they have no conflict of interest.

References

1. Jayaram S, Gupta MK, Polisetty RV, Cho WCS, Sirdeshmukh R (2014) Towards developing biomarkers for glioblastoma multiforme: a proteomics view. Expert Rev Proteomic 11:621–639
2. Stupp R, Hegi ME, Mason WP, van den Bent M, Taphoorn MJ, Janzer RC, Ludwin SK, Allgeier A, Fisher B, Belanger K, Hau P, Brandes AA, Gijtenbeek J, Marosi C, Vecht CJ, Mokhtari K, Wesseling P, Villa S, Eisenhauer E, Gorlia T, Weller M, Lacombe D, Cairncross JG, Mirimanoff RO, European Organisation for Research and Treatment of Cancer Brain Tumour and Radiation Oncology Groups, National Cancer Institute of Canada Clinical Trials Group (2009) Effects of radiotherapy with concomitant and adjuvant temozolomide versus radiotherapy alone on survival in glioblastoma in a randomised phase III study: 5-year analysis of the EORTC-NCIC trial. Lancet Oncol 10:459–466
3. Vidiri A, Pace A, Fabi A, Maschio M, Latagliata G, Anelli V, Piludu F, Carapella C, Giovinazzo G, Marzi S (2012) Early perfusion changes in patients with recurrent high-grade brain tumor treated with bevacizumab: preliminary results by a quantitative evaluation. J Exp Clin Cancer Res 31:33
4. Keunen O, Johansson M, Oudin A, Sanzey M, Rahim SAA, Fack F, Thorsen F, Taxt T, Bartos M, Jirik R, Miletic H, Wang J, Stieber D, Stuhr L, Moen I, Rygh CB, Bjerkvig R, Niclou SP (2011) Anti-VEGF treatment reduces blood supply and increases tumor cell invasion in glioblastoma. Proc Natl Acad Sci U S A 108:3749–3754
5. Kreisl TN, Kim L, Moore K, Duic P, Royce C, Stroud I, Garren N, Mackey M, Butman JA, Camphausen K, Park J, Albert PS, Fine HA (2009) Phase II trial of single-agent bevacizumab followed by bevacizumab plus irinotecan at tumor progression in recurrent glioblastoma. J Clin Oncol 27:740–745
6. Batchelor TT, Sorensen AG, di Tomaso E, Zhang WT, Duda DG, Cohen KS, Kozak KR, Cahill DP, Chen PJ, Zhu M, Ancukiewicz M, Mrugala MM, Plotkin S, Drappatz J, Louis DN, Ivy P, Scadden DT, Benner T, Loeffler JS, Wen PY, Jain RK (2007) AZD2171, a pan-VEGF receptor tyrosine kinase inhibitor, normalizes tumor vasculature and alleviates edema in glioblastoma patients. Cancer Cell 11:83–95
7. Yan H, Parsons DW, Jin G, McLendon R, Rasheed BA, Yuan W, Kos I, Batinic-Haberle I, Jones S, Riggins GJ, Friedman H, Friedman A, Reardon D, Herndon J, Kinzler KW, Velculescu VE, Vogelstein B, Bigner DD (2009) Mutations in gliomas. N Engl J Med 360:765–773
8. Port RE, Bernstein LJ, Barboriak DP, Xu L, Roberts TP, van Bruggen N (2010) Noncompartmental kinetic analysis of DCE-MRI data from malignant tumors: application to glioblastoma treated with bevacizumab. Magn Reson Med 64:408–417
9. Wen PY, Macdonald DR, Reardon DA, Cloughesy TF, Sorensen AG, Galanis E, DeGroot J, Wick W, Gilbert MR, Lassman AB, Tsien C, Mikkelsen T, Wong ET, Chamberlain MC, Stupp R, Lamborn KR, Vogelbaum MA, van den Bent MJ, Chang SM (2010) Updated response assessment criteria for high-grade gliomas: response assessment in neuro-oncology working group. J Clin Oncol 28:1963–1972
10. Ellingson BM, Wen PY, Cloughesy TF (2017) Modified criteria for radiographic response assessment in glioblastoma clinical trials. Neurotherapeutics 14:307–320
11. Norden AD, Drappatz J, Muzikansky A, David K, Gerard M, McNamara MB, Phan P, Ross A, Kesari S, Wen PY (2009) An exploratory survival analysis of anti-angiogenic therapy for recurrent malignant glioma. J Neuro-Oncol 92:149–155
12. Friedman HS, Prados MD, Wen PY, Mikkelsen T, Schiff D, Abrey LE, Yung WKA, Paleologos N, Nicholas MK, Jensen R, Vredenburgh J, Huang J, Zheng M, Cloughesy T (2009) Bevacizumab alone and in combination with irinotecan in recurrent glioblastoma. J Clin Oncol 27:4733–4740
13. Sathornsumetee S, Cao Y, Marcello JE, Herndon JE II, McLendon RE, Desjardins A, Friedman HS, Dewhirst MW, Vredenburgh JJ, Rich JN (2008) Tumor angiogenic and hypoxic profiles predict radiographic response and survival in malignant astrocytoma patients treated with bevacizumab and irinotecan. J Clin Oncol 26:271–278
14. Ebos JML, Lee CR, Kerbel RS (2009) Tumor and host-mediated pathways of resistance and disease progression in response to antiangiogenic therapy. Clin Cancer Res 15:5020–5025
15. Bergers G, Hanahan D (2008) Modes of resistance to anti-angiogenic therapy. Nat Rev Cancer 8:592–603
16. De Groot JF, Fuller G, Kumar AJ et al (2010) Tumor invasion after treatment of glioblastoma with bevacizumab: radiographic and pathologic correlation in humans and mice. Neuro-Oncology 12:233–242
17. Fack F, Espedal H, Keunen O, Golebiewska A, Obad N, Harter PN, Mittelbronn M, Bähr O, Weyerbrock A, Stuhr L, Miletic H, Sakariassen PØ, Stieber D, Rygh CB, Lund-Johansen M, Zheng L, Gottlieb E, Niclou SP, Bjerkvig R (2015) Bevacizumab treatment induces metabolic adaptation toward anaerobic metabolism in glioblastomas. Acta Neuropathol 129:115–131. https://doi.org/10.1007/s00401-014-1352-5

18. Hambardzumyan D, Bergers G (2015) Glioblastoma: defining tumor niches. Trends Cancer 1:252–265
19. Quail DF, Joyce JA (2017) The microenvironmental landscape of brain tumors. Cancer Cell 31:326–341
20. Greaves M, Maley CC (2012) Clonal evolution in cancer. Nature 481:306–313
21. Huse JT, Holland EC (2010) Targeting brain cancer: advances in the molecular pathology of malignant glioma and medulloblastoma. Nat Rev Cancer 10:319–331
22. Gillies RJ, Verduzco D, Gatenby RA (2012) Evolutionary dynamics of carcinogenesis and why targeted therapy does not work. Nat Rev Cancer 12:487–493
23. Marusyk A, Almendro V, Polyak K (2012) Intra-tumour heterogeneity: a looking glass for cancer? Nat Rev Cancer 12:323–334
24. Stadlbauer A, Zimmermann M, Doerfler A et al (2018) Intratumoral heterogeneity of oxygen metabolism and neovascularization uncovers 2 survival-relevant subgroups of IDH1 wild-type glioblastoma. Neuro Oncol. https://doi.org/10.1093/neuonc/noy066
25. Stadlbauer A, Zimmermann M, Oberndorfer S et al (2017) Vascular hysteresis loops and vascular architecture mapping in patients with glioblastoma treated with antiangiogenic therapy. Sci Rep 7:1–12
26. Stadlbauer A, Zimmermann M, Kitzwögerer M, Oberndorfer S, Rössler K, Dörfler A, Buchfelder M, Heinz G (2017) MR imaging–derived oxygen metabolism and neovascularization characterization for grading and IDH gene mutation detection of gliomas. Radiology 283:799–809
27. Stadlbauer A, Zimmermann M, Heinz G, Oberndorfer S, Doerfler A, Buchfelder M, Rössler K (2017) Magnetic resonance imaging biomarkers for clinical routine assessment of microvascular architecture in glioma. J Cereb Blood Flow Metab 37:632–643
28. Prasloski T, Mädler B, Xiang QS, MacKay A, Jones C (2012) Applications of stimulated echo correction to multicomponent T2 analysis. Magn Reson Med 67:1803–1814
29. Smith AM, Grandin CB, Duprez T et al (2000) Whole brain quantitative CBF, CBV, and MTT measurements using MRI bolus tracking: implementation and application to data acquired from hyperacute stroke patients. J Magn Reson Imaging 12:400–410
30. Bjornerud A, Emblem KE (2010) A fully automated method for quantitative cerebral hemodynamic analysis using DSC-MRI. J Cereb Blood Flow Metab 30:1066–1078
31. Christen T, Schmiedeskamp H, Straka M, Bammer R, Zaharchuk G (2012) Measuring brain oxygenation in humans using a multiparametric quantitative blood oxygenation level dependent MRI approach. Magn Reson Med 68:905–911
32. Gjedde A (2002) Cerebral blood flow change in arterial hypoxemia is consistent with negligible oxygen tension in brain mitochondria. Neuroimage 17:1876–1881
33. Vafaee MS, Vang K, Bergersen LH, Gjedde A (2012) Oxygen consumption and blood flow coupling in human motor cortex during intense finger tapping: implication for a role of lactate. J Cereb Blood Flow Metab 32:1859–1868
34. Boxerman JL, Schmainda KM, Weisskoff RM (2006) Relative cerebral blood volume maps corrected for contrast agent extravasation significantly correlate with glioma tumor grade, whereas uncorrected maps do not. Am J Neuroradiol 27:859–867
35. Boxerman JL, Prah DE, Paulson ES, Machan JT, Bedekar D, Schmainda KM (2012) The role of preload and leakage correction in gadolinium-based cerebral blood volume estimation determined by comparison with MION as a criterion standard. Am J Neuroradiol 33:1081–1087
36. Ducreux D, Buvat I, Meder JF, Mikulis D, Crawley A, Fredy D, TerBrugge K, Lasjaunias P, Bittoun J (2006) Perfusion-weighted MR imaging studies in brain hypervascular diseases: comparison of arterial input function extractions for perfusion measurement. AJNR Am J Neuroradiol 27:1059–1069
37. Xu C, Kiselev VG, Möller HE, Fiebach JB (2013) Dynamic hysteresis between gradient echo and spin echo attenuations in dynamic susceptibility contrast imaging. Magn Reson Med 69:981–991
38. Jensen JH, Lu H, Inglese M (2006) Microvessel density estimation in the human brain by means of dynamic contrast-enhanced echo-planar imaging. Magn Reson Med 56:1145–1150
39. Jain RK, Duda DG, Clark JW, Loeffler JS (2006) Lessons from phase III clinical trials on anti-VEGF therapy for cancer. Nat Clin Pract Oncol 3:24–40
40. Plate KH, Scholz A, Dumont DJ (2012) Tumor angiogenesis and anti-angiogenic therapy in malignant gliomas revisited. Acta Neuropathol 124:763–775
41. Arrillaga-Romany I, Reardon DA, Wen PY (2014) Current status of antiangiogenic therapies for glioblastomas. Expert Opin Investig Drugs 23:199–210
42. Hamans B, Navis AC, Wright A, Wesseling P, Heerschap A, Leenders W (2013) Multivoxel1h mr spectroscopy is superior to contrast-enhanced MRI for response assessment after anti-Angiogenic treatment of orthotopic human glioma xenografts and provides handles for metabolic targeting. Neuro-Oncology 15:1615–1624
43. Demeure K, Fack F, Duriez E, Tiemann K, Bernard A, Golebiewska A, Bougnaud S, Bjerkvig R, Domon B, Niclou SP (2016) Targeted proteomics to assess the response to anti-angiogenic treatment in human glioblastoma (GBM). Mol Cell Proteomics 15:481–492
44. Najafi M, Soltanian-Zadeh H, Jafari-Khouzani K, Scarpace L, Mikkelsen T (2012) Prediction of glioblastoma multiform response to bevacizumab treatment using multi-parametric MRI. PLoS One 7:e29945
45. Nowosielski M, Recheis W, Goebel G, Güler Ö, Tinkhauser G, Kostron H, Schocke M, Gotwald T, Stockhammer G, Hutterer M (2011) ADC histograms predict response to anti-angiogenic therapy in patients with recurrent high-grade glioma. Neuroradiology 53:291–302
46. Rahman R, Hamdan A, Zweifler R, Jiang H, Norden AD, Reardon DA, Mukundan S, Wen PY, Huang RY (2014) Histogram analysis of apparent diffusion coefficient within enhancing and nonenhancing tumor volumes in recurrent glioblastoma patients treated with bevacizumab. J Neuro-Oncol 119:149–158